Jurnal Ilmu dan Teknologi Kelautan Tropis

p-ISSN: 2087-9423
e-ISSN: 2620-309X

Wind-Driven Upwelling Dynamics in the Southwest Arafura Sea

Nabila Nur Hanifah[a], I Wayan Nurjaya [b],Yuli Naulita[b], Nyoman M. N. Natih [b]

[a] Magister program of Marine Science, Faculty of Fishery and Marine Science, IPB University, Dramaga Campus, Bogor 16680, Indonesia

[b] Department of Marine Science and Technology, Faculty of Fishery and Marine Science, IPB University, Dramaga Campus, Bogor 16680, Indonesia

Article Info:
Received 27 November 2025
Revised 23 January 2026
Accepted 03 February 2026

Corresponding Author:
Nabila Nur Hanifah
Magister Program of Marine Science
IPB University
E-mail:1306nabila@apps.ipb.ac.id

Abstract

This study examines the spatial and temporal variability of upwelling in the southwestern Arafura Sea, focusing on the influence of monsoonal winds and ENSO variability. The objective is to identify the physical mechanisms driving upwelling formation in the region. Satellite-derived sea surface temperature (SST) and chlorophyll-a data from 2010, 2015, and 2020 were analyzed during the Southeast Monsoon (June–August). In addition, wind data, surface currents, Ekman Mass Transport (EMT), and Ekman Pumping Velocity (EPV) were evaluated to investigate the underlying oceanographic processes. The results indicate that intensified southeasterly winds during the Southeast Monsoon enhance offshore Ekman transport and generate negative wind stress curl, leading to significant Ekman pumping with EPV values reaching up to -2.1×10^{-5} m/s. These processes promote the upwelling of cooler, nutrient-rich subsurface waters, as reflected by decreased SST and increased chlorophyll-a concentrations. Conversely, weaker wind forcing reduces Ekman dynamics and weakens upwelling intensity. Vertical profiles further confirm thermocline shoaling and the upward displacement of subsurface waters during strong wind conditions. In conclusion, upwelling variability in the southwestern Arafura Sea is primarily controlled by seasonal monsoonal winds and large-scale climate variability, while regional circulation, such as the Indonesian Throughflow, contributes to the availability of cooler subsurface water that enhances surface cooling when uplifted by Ekman processes.

Keywords: Arafura Sea, Ekman Transport, Ekman Pumping, Upwelling

1. Introduction

The Arafura Sea is one of Indonesia's most productive marine regions, largely influenced by seasonal wind-driven upwelling processes. Upwelling occurs when physical oceanographic processes transport colder and nutrient-rich subsurface waters into the surface layer, enhancing primary productivity and increasing phytoplankton biomass as indicated by elevated chlorophyll-a concentrations (Rudiastuti et al., 2007). This process typically replaces warm, nutrient-depleted surface waters with colder nutrient-rich waters, thereby playing an important role in regulating marine ecosystem productivity.

Wind-driven circulation is one of the main mechanisms controlling upwelling through Ekman dynamics. Ekman transport refers to the horizontal movement of surface waters driven by wind stress and deflected perpendicular to the wind direction due to the Coriolis effect, while Ekman pumping represents the vertical velocity generated by divergence or convergence of Ekman transport, commonly estimated from wind stress curl (Bernades et al., 2021). These processes are fundamental in controlling vertical water movement and upper ocean heat distribution, particularly in upwelling regions (Talley et al., 2011; Kämpf and Chapman, 2016)

Previous studies have shown that sea surface temperature (SST) variability in upwelling regions is strongly influenced by wind-driven processes; however, the specific contributions of Ekman Mass Transport (EMT) and Ekman Pumping Velocity (EPV) to SST and biological variability have received less attention, particularly in the Arafura Sea (Bernades et al., 2021). Coastal upwelling may also be generated by alongshore winds that induce offshore Ekman transport, allowing deeper nutrient-rich waters to rise to the surface (Kämpf and Chapman, 2016). Numerical modeling by Kämpf (2015) further demonstrated that during

the southeast monsoon, undercurrent formation associated with lee-effect dynamics can transport nutrient-rich waters from the Banda Sea toward the Arafura shelf, which may subsequently be lifted to the surface through wind-driven upwelling processes.

Regional circulation variability also contributes to the complexity of ocean dynamics in the Arafura Sea. Surface geostrophic currents in the Arafura–Timor region are strongly influenced by monsoonal wind regimes, which can generate surface divergence and enhance upwelling potential along the continental shelf (Ramadyan and Radjawane, 2013). In addition, climate variability associated with the El Niño–Southern Oscillation (ENSO) has been shown to influence oceanographic conditions in the Arafura Sea. Observations by Wattimena and Tubalawony (2023) showed lower SST and sea level height during the 2015 super El Niño event, while increased salinity and mixed layer thickness were observed during the 2010 La Niña event. Strengthening of subsurface eastward currents along the northern Arafura slope during the southeast monsoon was also found to be more pronounced during El Niño compared to La Niña conditions.

The southwestern Arafura Sea is important for studying oceanographic processes, for it is highly productive and sensitive to regional climate change (Buton et al., 2023). Studies show that both the Arafura and Timor Seas experience upwelling and downwelling throughout the year, mainly due to strong monsoons (Pranowo, 2012). During the southeast monsoon, negative sea surface temperature (SST) anomalies in the northern Arafura Sea are linked to seasonal upwelling (Kida and Wijffels, 2012).

A comprehensive understanding of the simultaneous influence of wind-driven Ekman processes on both physical and biological responses in the southwestern Arafura Sea remains limited. Most prior research has addressed sea surface temperature (SST) variability, circulation dynamics, or climate variability in isolation. Integrated analyses that connect Ekman Mass Transport (EMT), Ekman Pumping Velocity (EPV), SST variability, and chlorophyll-a responses are rare, especially at seasonal and interannual timescales. This gap limits understanding of the coupled physical and biological mechanisms regulating upwelling intensity in the region.

This study investigates the roles of Ekman Mass Transport and Ekman Pumping Velocity in regulating upwelling variability in the southwestern Arafura Sea, with a focus on their effects on SST cooling and chlorophyll-a enhancement during the southeast monsoon. An integrated analysis of atmospheric forcing, oceanic response, and biological indicators is presented to elucidate the mechanisms governing upwelling variability in the Arafura continental shelf system.

2. Materials and Methods

2.1. Study Area

Observations were conducted to determine the presence and potential of upwelling in the southwestern Arafura Sea (longitude: 130°E – 132°E and latitude: 7.8°S – 9.2°S). This region is directly influenced by the seasonal monsoon system and outflow of the Indonesian Throughflow (ITF). Unlike most previous studies, which predominantly focused on upwelling dynamics in the northwestern Arafura Sea, the southwestern sector remains comparatively underexplored. Limited investigations in this area highlight the need for more detailed assessments, particularly regarding its hydrographic variability and the possible emergence of localized upwelling features. **Figure 1** shows the study area with stations from CTD observations, which will be used for validation of the reanalysis data.

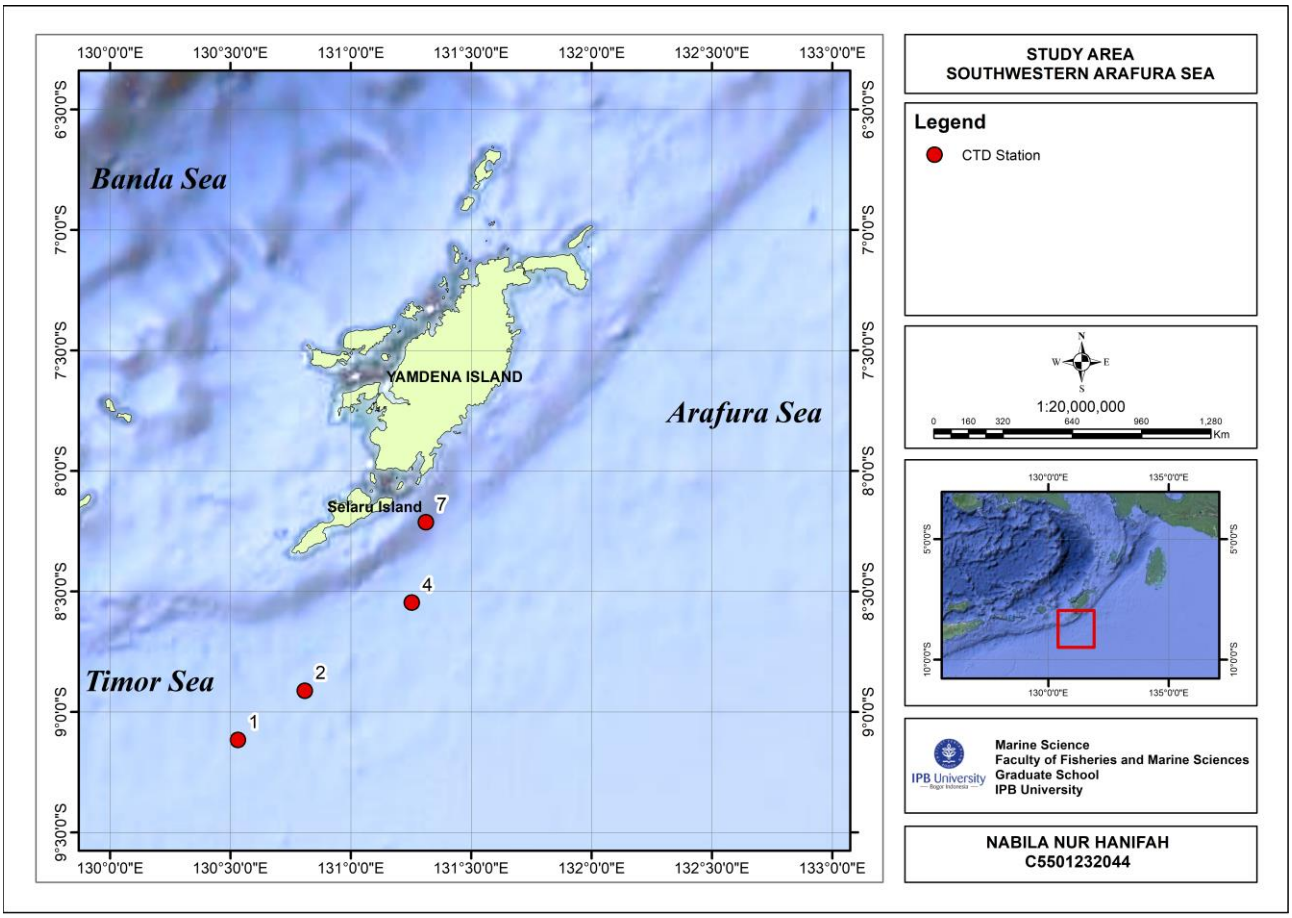

Figure 1. Study area in the southwestern Arafura Sea showing the locations of CTD stations surveyed during the oceanographic survey conducted by Inpex Masela Ltd in the Abadi Field. The CTD measurements provide in-situ vertical profiles of seawater temperature, which are used to characterize the hydrographic conditions of the region. Among the numerous CTD stations obtained during the survey, Station 7 was selected as the reference station for validating satellite-derived sea surface temperature data, as its location coincides with the corresponding satellite grid point.

2.2. Data

The observation period focused on the eastern monsoon, specifically from June to August, and the reference years were selected based on the Niño 3.4 index. The years analyzed were 2010 (La Niña), 2015 (El Niño), and 2020 (neutral/normal conditions). The data used included sea surface temperature (SST) data obtained from the Operational Sea States Time Inversion Application (OSTIA) product downloaded in NetCDF format through Copernicus Marine Environment Monitoring Service (CMEMS with DOI: https://doi.org/10.48670/moi-00165, in the form of daily data, with a DOI of https://doi. org/10.48670/moi-00165. The data were available on a daily basis and were subsequently averaged over months with a resolution of 0.05° × 0.05°. Chlorophyll-a data with a spatial resolution of 4 × 4 km were downloaded from CMEMS in NetCDF format DOI https://doi.org/10.48670/moi-00283) and had a monthly temporal resolution. Additional supporting data included wind fields in the form of zonal (U) and meridional (V) components downloaded from CMEMS (https://doi.org/10.48670/moi-00181) at a spatial resolution of 0.25°. These wind data were used to calculate Ekman transport and Ekman pumping. Several programs, such as PyFerret, Python, and JupyterLab Notebook, were used for data processing and analysis, as well as for visualization. SST datasets were validated against combined tomography and deep sounding (CTD) observations collected in the study area using the Taylor diagram method, as shown in **Figure 2.**

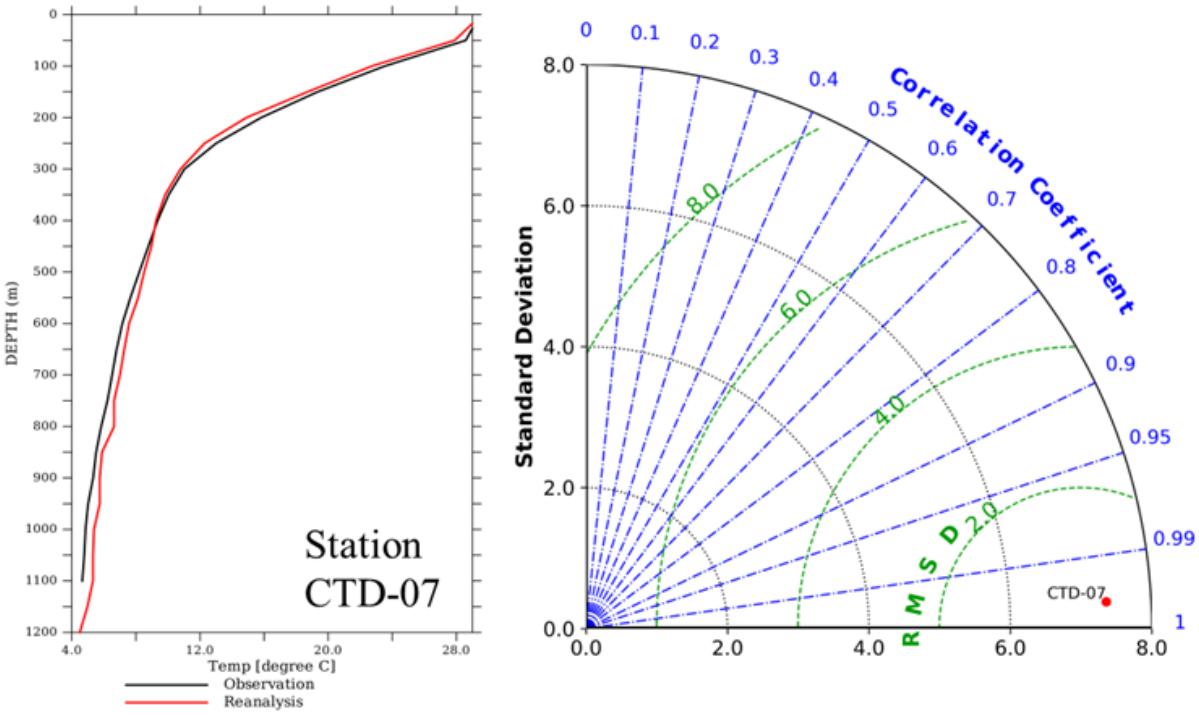

Figure 2. Sea surface temperature (SST) data from OSTIA were validated against in situ CTD measurements collected in the study area using the Taylor diagram method. The validation results indicate strong consistency between OSTIA SST and observational data, supporting the use of OSTIA SST as a representative dataset for surface thermal conditions in the study area.

Station 7 was selected as the reference station, where the observational data exhibited a standard deviation of 6.99, a correlation coefficient of 1.00, and a centered root-mean-square difference (CRMSD) of 0.00, whereas the reanalysis data showed a standard deviation of 7.37, a correlation coefficient of 0.9987, and a CRMSD of 0.53. The similarity in the correlation coefficient and low CRMSD indicated excellent correspondence between the reanalysis and in situ measurements, confirming that the reanalysis data were representative of the observed conditions.

2.3. Method

The occurrence of upwelling can be quantitatively assessed through Ekman dynamics, particularly using Ekman mass transport (*EMT*) and Ekman pumping velocity (*EPV*), which together describe the wind-driven horizontal transport and vertical motion of the upper ocean. These parameters are fundamentally governed by the interaction between surface winds and the Coriolis force.

Wind stress, which serves as the primary forcing mechanism for *EMT* and *EPV*, was computed based on the formulation of Rachman et al. (2019). As described by Ratnawati et al. (2016), the x-component (zonal) of the wind is parallel to the coastline, and the y-component (meridional) is perpendicular. The wind stress components are calculated as follows:

$$\tau_y = \rho_a C_d (U_w^2 + V_w^2)^{1/2} V_w \text{ and } \tau_x = \rho_a C_d (U_w^2 + V_w^2)^{1/2} U_w \quad (1)$$

The variables τ_x and τ_y represent the zonal and meridional wind stress components (N m^{-2}), respectively; ρ_a is air density (1.22 kg m^{-3}); C_d is the drag coefficient (1.4 × 10^{-3}); and W_x and W_y are the zonal and meridional wind speed components (m/s^{-1}), respectively.

The Coriolis parameter (f), which influences both the direction and magnitude of Ekman transport $f=2\Omega sin\theta$. Using f as the Coriolis parameter (rad s^{-1}), Ω is Earth's angular velocity (7.29 × 10^{-5} rad s^{-1}), and θ is the latitude.

The Ekman mass transport (*EMT*) describes the net horizontal transport of surface water driven by wind stress and modified by Coriolis forcing. According to Wirasatriya et al. (2020), *EMT* is computed as follows:

$$EMT = \frac{\tau}{\rho_w f} \tag{2}$$

where τ is the wind stress vector, ρ_w is the seawater density (1025 kg m^{-3}), Ekman Pumping Velocity (*EPV*), which characterizes the vertical movement of water masses, and is calculated using the wind stress curl, which is obtained from the rotational component of wind stress. *EPV* is expressed as:

$$EPV = \frac{curl}{\rho_w f} \tag{3}$$

where wind stress curl is defined as follows:

$$curl = -\frac{\partial \tau_y}{\partial x} - \frac{\partial \tau_x}{\partial y} \tag{4}$$

where curl represents the wind stress curl vector, and τ_x and τ_y are the zonal and meridional wind stress components, respectively.

Together, *EMT* and *EPV* provide a comprehensive representation of the horizontal divergence and vertical displacement of water masses associated with upwelling. Positive *EPV* values (upward motion) and divergence-driven *EMT* patterns are key indicators of the upwelling phenomenon in the Arafura Sea.

3. Results and Discussion

3.1. Wind Patterns and Surface Current Dynamics

Surface wind patterns in the southwestern Arafura Sea play a crucial role in regulating seasonal ocean dynamics. During the Northwest Monsoon (February 2020), winds were predominantly northwesterly, moving southeastward at approximately 7.03 m/s. Wind vectors remained relatively uniform but weakened near coastal zones, indicating limited potential for significant surface water divergence. This pattern is consistent with the general characteristics of the northwest monsoon, which is typically weaker than the southeast monsoon in tropical regions (Clark et al., 2000). **Figure 3** shows the seasonal wind vector fields during JJA, highlighting strong southeasterly winds that favor offshore Ekman transport and upwelling processes.

In contrast, during the Southeast Monsoon (July 2020), winds consistently originated from the southeast and moved toward the northwest, with speeds up to 8.8 m/s. These stronger winds enhance the potential for offshore Ekman transport and surface divergence, which may act as an initial driver of upwelling processes in the study area. Seasonal variability is evident in surface current patterns, which generally correspond to wind dynamics. Surface current speeds ranged from approximately 0.1 to 0.25 m/s, with weaker currents during the Northwest Monsoon and stronger currents during the Southeast Monsoon. These low current magnitudes are typical of shallow shelf seas such as the Arafura Sea, where strong bottom friction limits the acceleration of surface currents (Kämpf, 2015). **Figure 4** shows the spatial distribution of surface currents during JJA, demonstrating circulation patterns influenced by monsoonal winds**.**

Seasonal variability is evident in surface current patterns, which generally correspond to wind dynamics. Surface current speeds ranged from approximately 0.1 to 0.25 m/s, with weaker currents during the Northwest Monsoon and stronger currents during the Southeast Monsoon. These low current magnitudes are typical of shallow shelf seas such as the Arafura Sea, where strong bottom friction limits the acceleration of surface currents (Kämpf, 2015).

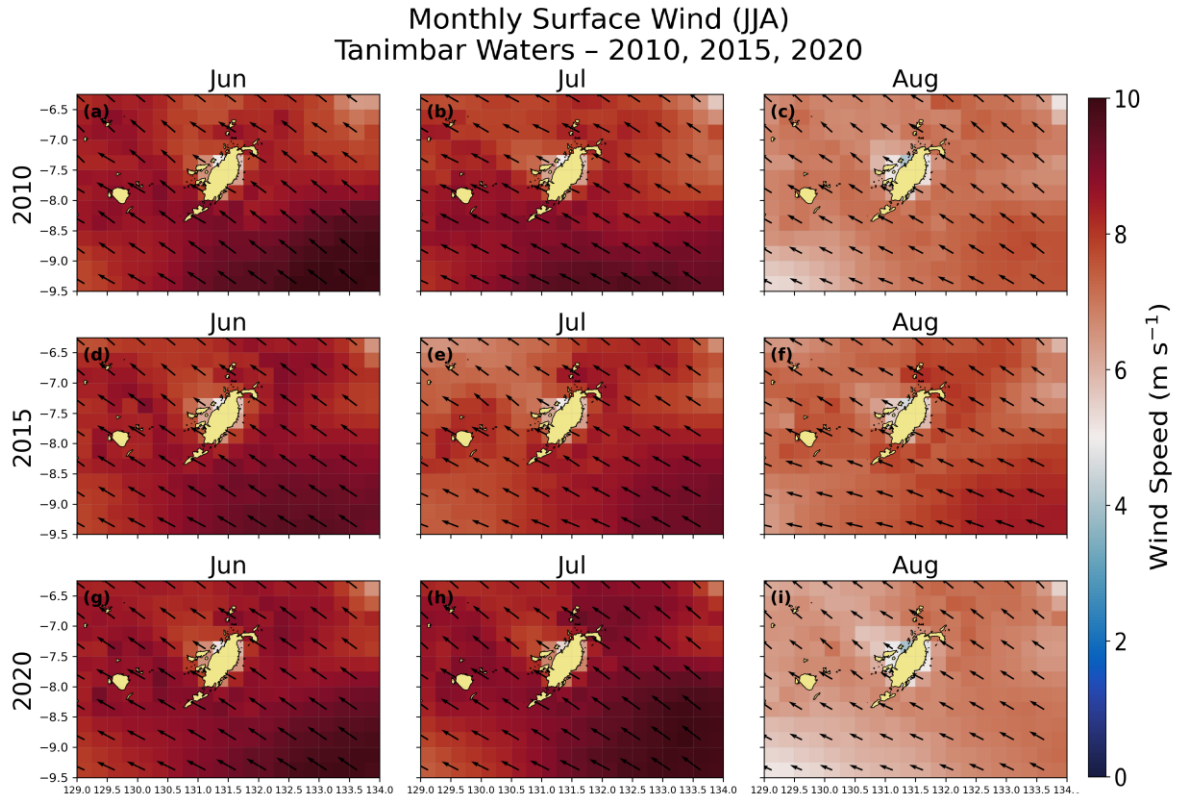

Figure 3. Seasonal wind vector fields during JJA for 2010 (a-c), 2015 (d-f), and 2020 (g-i). The strong southeasterly winds in JJA are consistent with conditions favorable for offshore Ekman transport and wind-driven upwelling along the southwest Arafura shelf.

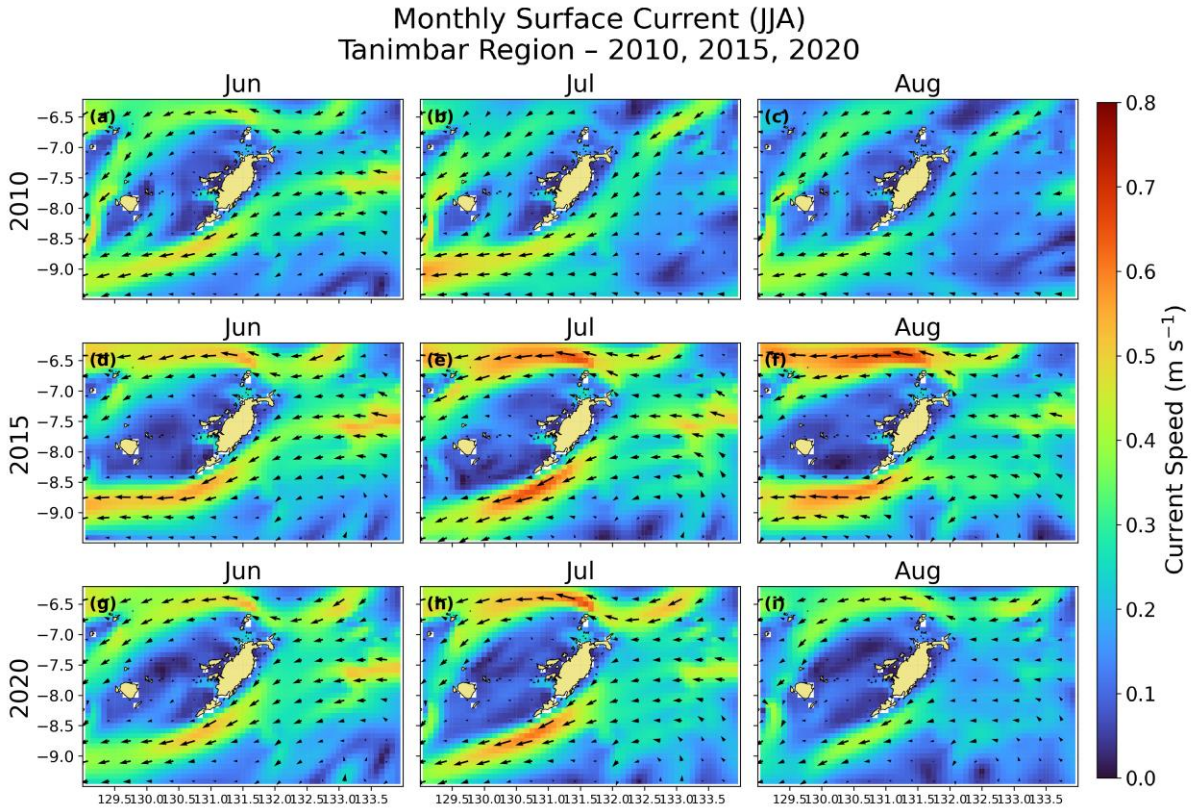

Figure 4. Spatial distribution of surface currents during JJA for 2010 (a-c), 2015 (d-f), and 2020 (g-i). Current direction aligned with monsoonal wind and cross-shelf circulation, modulating surface divergence and stratification.

In February 2020, surface currents were relatively weak (0.15 m/s) and less organized, indicating limited surface mass transport. By July 2020, currents became more organized and intensified to approximately 0.25 m/s, consistent with stronger southeast monsoon winds. Current patterns also reveal eddy structures near the Tanimbar Islands, as reported by Ramadyan and Radjawane (2013). The intensification of surface currents during the Southeast Monsoon demonstrates the ocean's response to stronger wind forcing, which may enhance surface divergence and promote upwelling processes. These circulation patterns affect the distribution of physical and biological properties, particularly sea surface temperature (SST) and chlorophyll-a.

These seasonal differences in wind and current dynamics indicate distinct ocean responses between monsoons. To further examine how these physical forcings influence ocean surface conditions, the spatial variability of sea surface temperature (SST) and chlorophyll-a is analysed in the following section.

3.2. Spatial Variability of Sea Surface Temperature (SST) and Chlorophyll-a

The spatial distributions of sea surface temperature (SST) and chlorophyll a were examined for February and July 2020, which correspond to the Northwest and Southeast Monsoon periods, respectively, under neutral climate conditions. Selecting a neutral year minimized the influence of interannual climate variability and allowed for clearer isolation of the seasonal monsoonal signal. In February 2020, SST distribution was relatively homogeneous, indicating stable surface water conditions without significant localized cooling. The average SST was 29.58 °C, with a maximum of 30.04 °C. Chlorophyll-a concentration remained low, averaging 0.18 mg/m³ and reaching a maximum of 5.81 mg/m³, suggesting limited nutrient supply to the surface layer. **Figure 5** shows the spatial distribution of sea surface temperature during JJA, indicating clear cross-shelf thermal gradients associated with seasonal forcing.

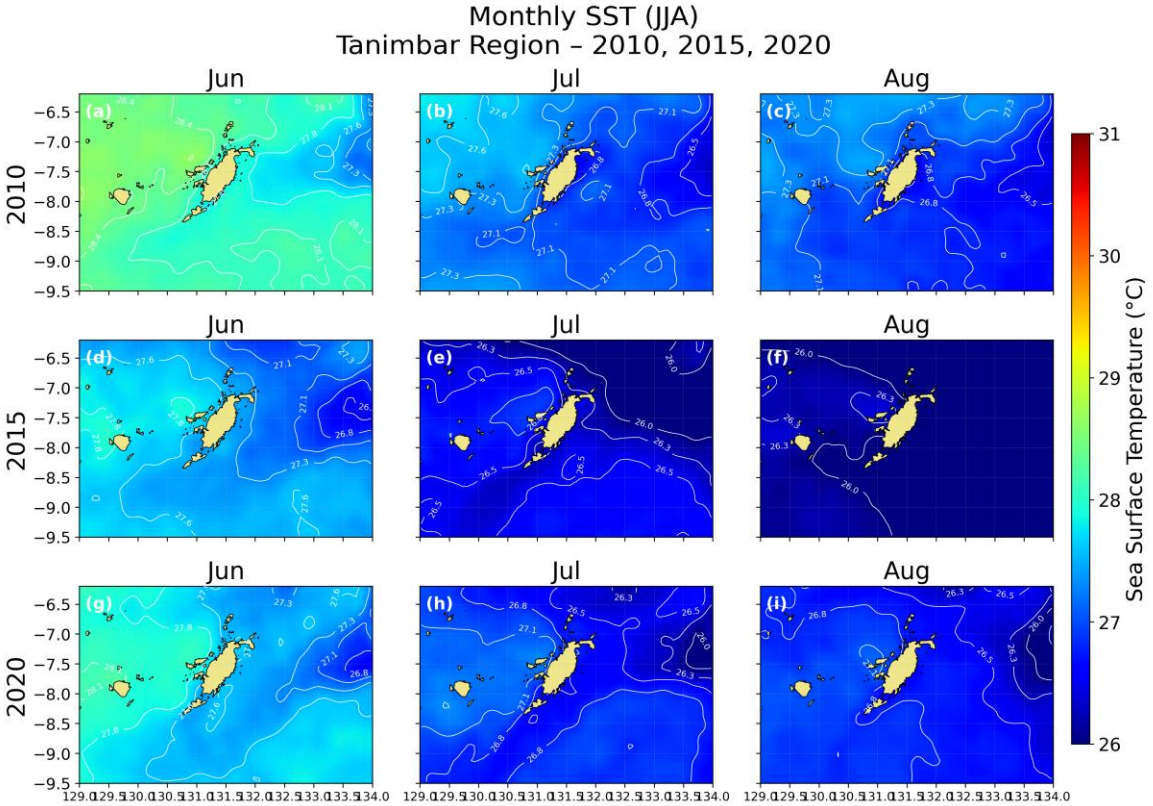

Figure 5. The spatial distribution of sea surface temperature (SST) during JJA for 2010 (a-c), 2015 (d-f), and 2020 (g-i) displays clear spatial variability characterized by cross-shelf temperature gradients and regional contrasts, indicating the role of monsoonal conditions in shaping surface thermal patterns.

This condition is likely due to the intrusion of warmer waters from the Indonesian Throughflow (ITF), which suppresses surface cooling and reduces the potential for upwelling. In July 2020, SST showed cooler zones across parts of the study area, with an average temperature of 26.78 °C, a maximum of 27.32 °C, and a minimum of 25.82 °C. This cooling coincided with increased chlorophyll-a concentration, averaging 0.53 mg/m³ and reaching a maximum of 6.26 mg/m³. **Figure 6** shows the spatial distribution of chlorophyll-a during JJA, with higher concentrations corresponding to areas of lower SST.

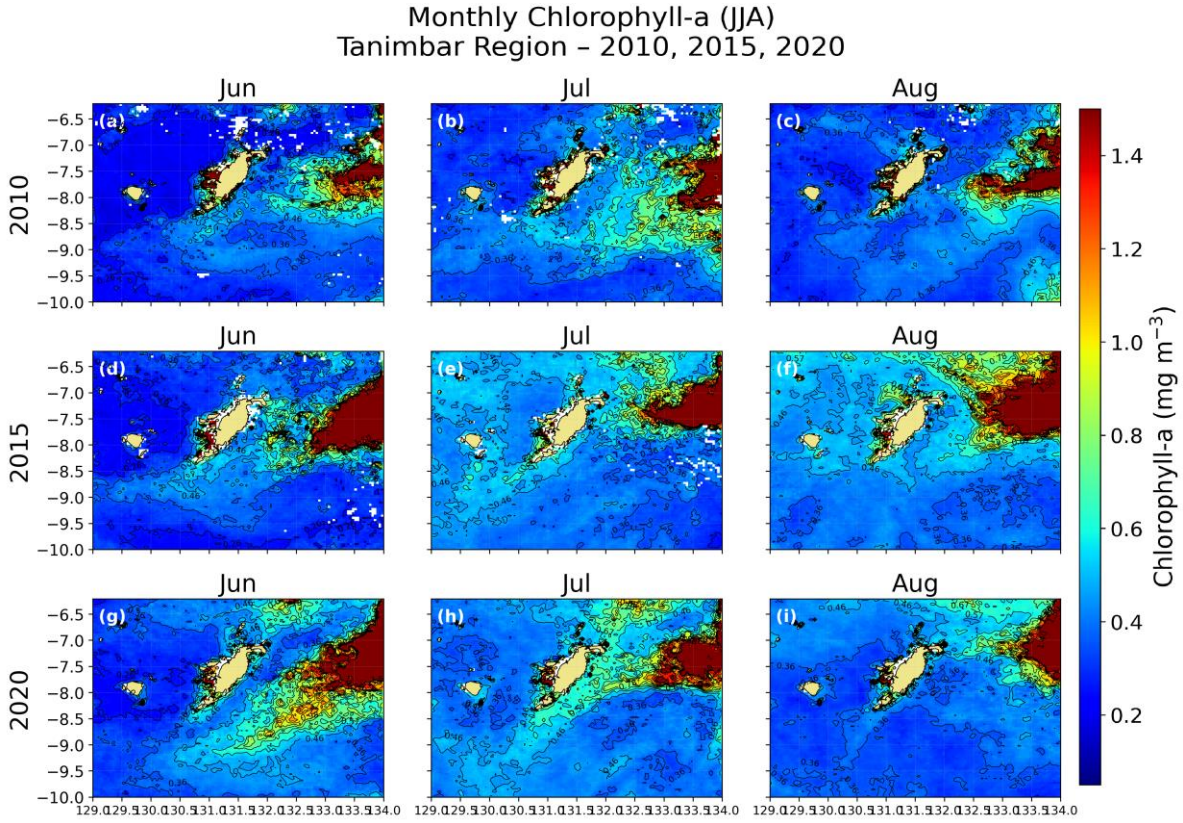

Figure 6. During JJA for 2010 (a-c), 2015 (d-f), and 2020 (g-i), Chlorophyll-a concentrations were highest in areas with SST cooling, indicating increased nutrient supply driven by monsoonal forcing.

The simultaneous presence of lower SST and higher chlorophyll-a suggests enhanced primary productivity, likely resulting from the upward transport of nutrient-rich subsurface waters during the Southeast Monsoon. These seasonal differences in SST and chlorophyll-a distributions demonstrate variability in water mass characteristics driven by monsoonal forcing. The co-occurrence of SST cooling and increased chlorophyll-a during the Southeast Monsoon suggests enhanced vertical nutrient supply. To further verify this indication, the vertical structure of temperature and chlorophyll-a is examined in the next section.

3.3. Vertical Profiles of Temperature and Chlorophyll-a

Vertical profiles of temperature (thetao) and chlorophyll-a were examined from the surface to 140 m to assess water-column structure and identify subsurface indicators of upwelling. Variations in these parameters serve as key indicators of thermocline depth and the vertical transport of nutrient-rich waters. The transect from point A (130.14°E, 9.35°S) to point B (132.29°E, 6.25°S) was chosen to represent the southwestern Arafura Sea and to capture the vertical response of the water column to seasonal ocean dynamics. **Figure 7** shows the vertical temperature structure along transect, illustrating the shoaling of isotherms associated with upwelling.

In February 2020, the vertical temperature structure was largely homogeneous, with temperatures at 50 m depth near 28 °C in the southwestern section and approximately 28.5 °C in the northeastern section. The vertical chlorophyll a profile was similarly uniform, with concentrations around 0.3 mg/m³ at depths of 60-70 m. These observations are consistent

with positive EPV values (1.12×10^{-6} m/s in the southwest and 6.33×10^{-6} m/s in the northeast), which indicate downwelling conditions that inhibit the upward transport of nutrients. This interpretation is further supported by low surface chlorophyll concentrations and elevated surface temperatures.

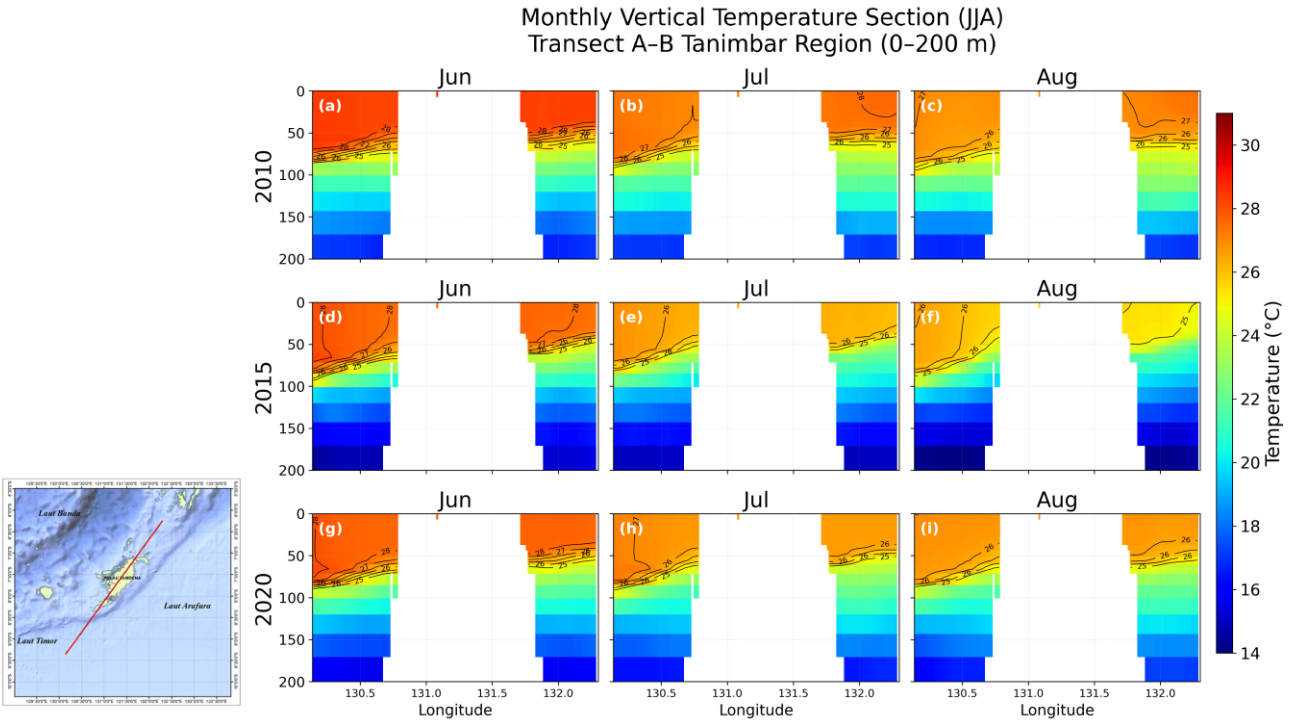

Figure 7. Vertical temperature profiles along transect during JJA for 2010 (a-c), 2015 (d-f), and 2020 (g-i) reveal a seasonal structure. Shoaling of isotherms indicates upward movement of cooler subsurface water due to wind-driven upwelling.

In contrast, during July 2020, the vertical structure exhibited significant changes, including a shallower thermocline and stronger vertical temperature gradients, particularly near the 26.5 °C isotherm. This pattern indicates enhanced vertical mixing and the upward movement of cooler subsurface waters. The vertical distribution of chlorophyll-a also showed higher concentrations at shallower depths, suggesting upwelling of nutrient-rich waters during the Southeast Monsoon. **Figure 8** shows the vertical chlorophyll-a distribution along the 8.2°S transect, highlighting a shallower deep chlorophyll maximum during JJA.

In July 2015, chlorophyll-a concentrations increased to approximately 0.4 mg/m³ and extended from depths of about 50 m to the surface in the southwestern transect. In the northeastern transect, chlorophyll-a reached around 0.5 mg/m³ from 50 m depth to the nearshore surface and remained relatively high below 50 m. By August 2015, chlorophyll-a concentrations further increased to 0.5-0.7 mg/m³, particularly near the coast along the southwestern transect, indicating greater seasonal variability compared to other years. The observed shoaling of the thermocline and increased subsurface chlorophyll during the Southeast Monsoon indicate enhanced vertical water movement. The following section analyses Ekman transport and Ekman pumping to elucidate the physical mechanisms underlying this process.

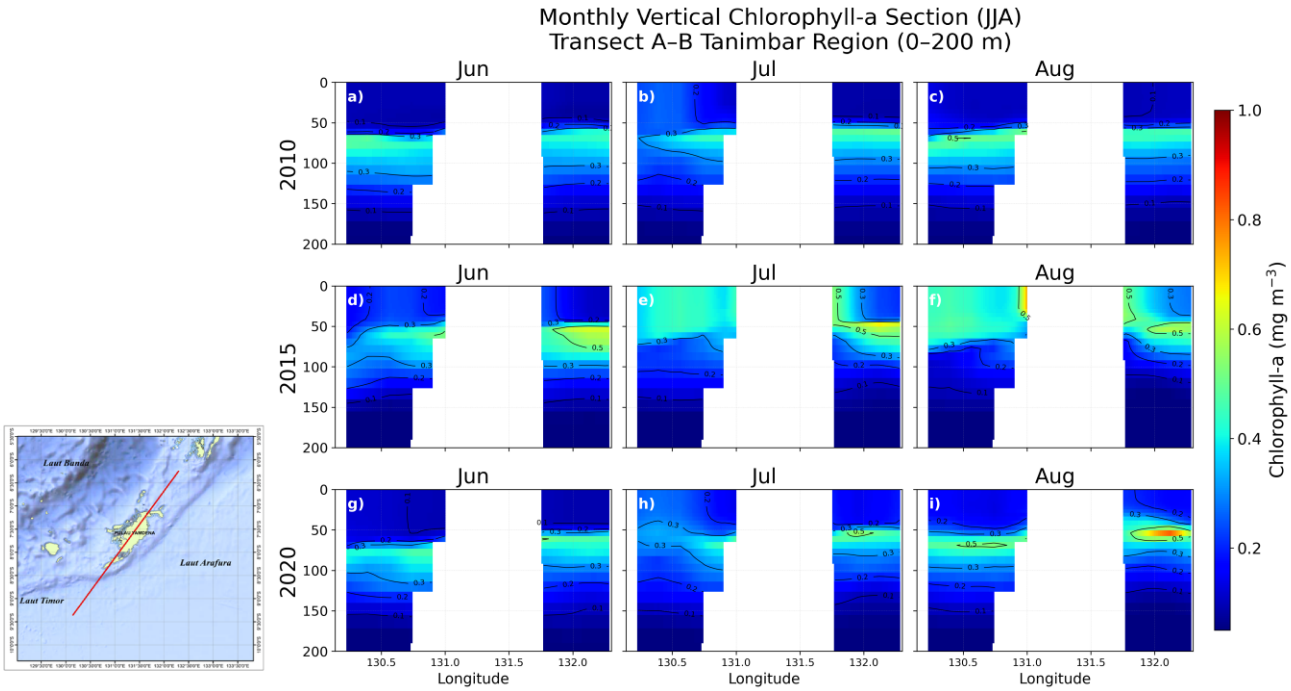

Figure 8. Vertical chlorophyll-a profiles along the 8.2°S slope transect during JJA for 2010 (a-c), 2015 (d-f), and 2020 (g-i) reveal a shallower deep chlorophyll maximum, suggesting increased nutrient input from below the thermocline.

3.4. Ekman Pumping Velocity and Upwelling Signatures

Upwelling characteristics were further examined using Ekman Mass Transport (EMT) and Ekman Pumping Velocity (EPV) to evaluate the strength and direction of wind-driven water mass movement. A transect between point A (130.14°E, 9.35°S) and point B (132.29°E, 6.25°S) was selected to analyse the relationship between Ekman dynamics, vertical temperature structure, and chlorophyll-a distribution. **Figure 9** shows the spatial distribution of Ekman pumping velocity during JJA, where negative values indicate upwelling conditions.

In February 2020, Ekman dynamics indicated downwelling conditions, as reflected by positive EPV values of 1.12×10^{-6} m/s in the southwestern area and 6.33×10^{-6} m/s in the northeastern area. Positive EPV values indicate surface water convergence and downward water movement. This condition is consistent with the Northwest Monsoon, when relatively weaker winds (7.03 m/s) and lower surface current speeds (0.15 m/s) provide limited forcing to generate significant Ekman-induced upwelling.

In contrast, during July 2020 EPV values became negative at the same locations, reaching -5×10^{-6} m/s in the southwestern region and -1.93×10^{-5} m/s in the northeastern region. These negative values indicate surface water divergence associated with the upward movement of deeper water masses. Considering Ekman transport characteristics in the Southern Hemisphere, where transport is directed to the left of the wind direction, these conditions support the development of upwelling during the Southeast Monsoon.

These findings are consistent with the observed SST cooling, increased chlorophyll-a concentrations, and the shoaling of the thermocline discussed in the previous sections, confirming that upwelling processes intensify during July. The simultaneous increase in wind speed (8.8 m/s) and surface current velocity (0.25 m/s) further demonstrates the strong influence of wind forcing on surface circulation and Ekman-driven upwelling in the study area.

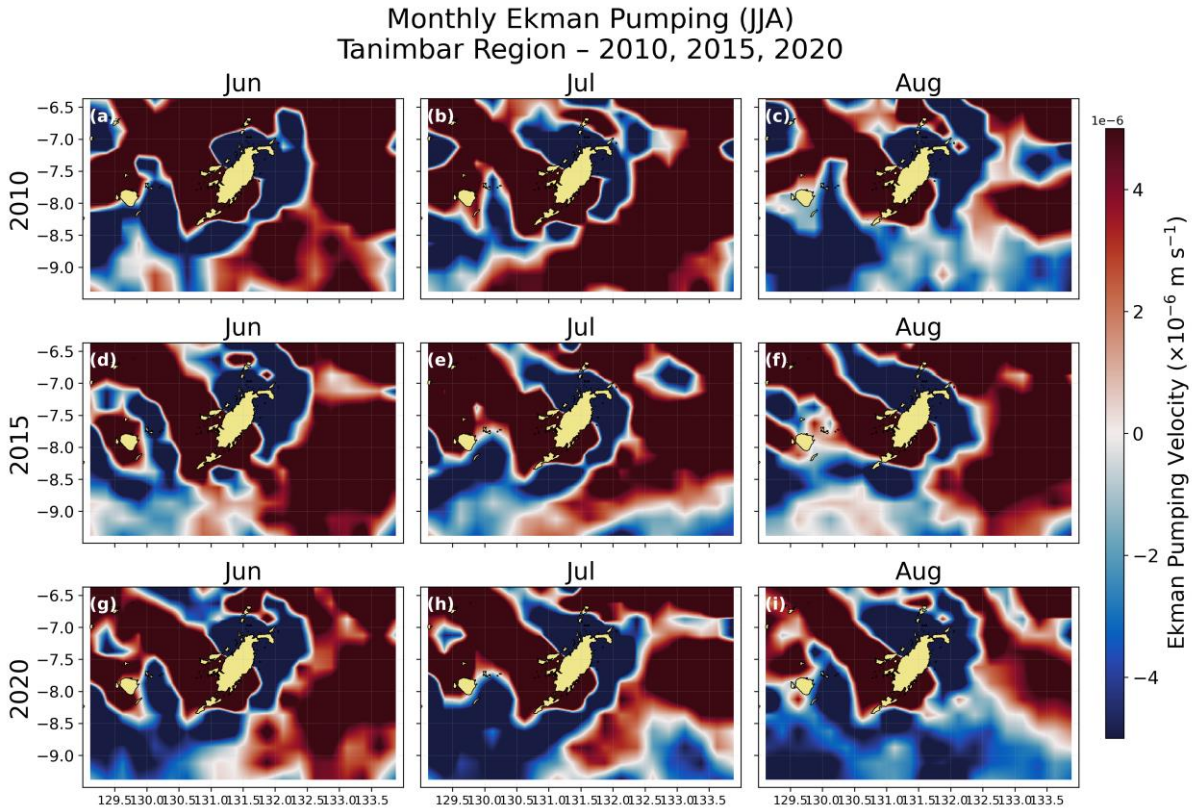

Figure 9. Shows the spatial distribution of the Ekman pumping velocity (EPV) during JJA for 2010 (a-c), 2015 (d-f), and 2020 (g-i). Negative EPV values, indicating upward motion, are most common during JJA and align with increased wind stress curl and stronger upwelling.

3.5. Discussion

The results of this study demonstrate a clear seasonal coupling between wind forcing, ocean circulation, and biological responses in the southwestern Arafura Sea. A similar approach was applied by a study published in JITKT by Atmadipoera et al. (2020), which examined upwelling characteristics in southern Java during the strong La Niña 2010 and the super El Niño 2015. The authors demonstrated that variations in upwelling intensity can be effectively assessed using wind-driven indices, such as Ekman transport and Ekman pumping. Intensified southeasterly winds during the Southeast Monsoon increased surface currents, offshore Ekman transport, and negative Ekman Pumping Velocity (EPV), collectively promoting the uplift of cooler, nutrient-rich subsurface waters. This process is evidenced by sea surface temperature (SST) cooling, elevated chlorophyll-a concentrations, and thermocline shoaling during the June–August (JJA) period, confirming the primary influence of wind-driven Ekman dynamics on seasonal upwelling variability and upper ocean productivity.

The observed seasonal wind variability underscores the Southeast Monsoon's significant role in regulating upper-ocean dynamics. According to Buton et al. (2023), prevailing southeasterly winds are associated with higher atmospheric pressure over the southeastern region compared to the western and northwestern areas, resulting in a persistent northwestward wind flow. During the Northwest Monsoon, weaker winds diminish vertical mixing and permit greater solar heating, leading to warmer SST (Arisandi et al., 2017). Conversely, stronger Southeast Monsoon winds intensify vertical mixing and surface divergence, resulting in lower SST, as demonstrated in the 2020 seasonal comparison.

Interannual variability among La Niña, El Niño, and neutral conditions further illustrates the impact of large-scale climate variability on regional oceanographic processes. Warmer SST and reduced chlorophyll concentrations during La Niña indicate weaker upwelling, likely resulting from increased stratification and a deeper thermocline. In contrast, cooler SST and moderately elevated chlorophyll concentrations during El Niño suggest enhanced vertical

nutrient transport. This observation aligns with Buton et al. (2023), who documented significant SST reductions during June–August in El Niño years, driven by large-scale redistribution of Pacific Ocean temperatures. Beyond ENSO forcing, regional factors such as cooler water advection from the Torres Strait and the presence of relatively dry air masses may also contribute to SST reduction.

Thermocline shoaling observed alongside increased chlorophyll concentrations provides compelling evidence for wind-driven upwelling. This pattern corresponds with negative EPV values, which indicate surface divergence and upward vertical transport. Comparable seasonal upwelling mechanisms in the Arafura Sea have been described by Kämpf (2015), where Southeast Monsoon winds and regional circulation, including inflow from the Banda Sea, contribute to nutrient enrichment of the upper ocean layer. The gradual SST cooling from June to August further substantiates the development of seasonal upwelling, especially in offshore southwestern areas.

The more pronounced upwelling signal observed in 2015 relative to 2010 and 2020 is supported by a greater negative EPV magnitude, indicating stronger surface divergence and more efficient vertical transport. This phenomenon is likely associated with El Niño variability, which can alter regional wind forcing and upper ocean stratification. The intensified Ekman response is further evidenced by greater SST cooling and signs of increased biological productivity, although spatial responses remain heterogeneous due to local circulation differences.

Beyond atmospheric forcing, the vertical structure of the water column significantly influences biological responses. The occurrence of a subsurface chlorophyll maximum during both normal and ENSO years indicates that phytoplankton growth depends on nutrient availability, light penetration, and stratification strength. Under moderate upwelling conditions, nutrient enrichment may primarily stimulate phytoplankton growth below the surface, where light remains adequate, which explains why chlorophyll enhancement in 2020 was dominated by subsurface maxima rather than the pronounced surface blooms observed in 2015.

Spatial contrasts between the southwestern and northeastern transects indicate that local circulation patterns and bathymetry modulate upwelling responses. Differences in shelf width, bottom topography, and current interactions can affect the efficiency of vertical transport and nutrient redistribution. These findings are consistent with previous studies demonstrating that continental shelf morphology strongly influences the spatial variability of upwelling intensity and productivity.

The intensified biological response observed in 2015 may also result from upper ocean preconditioning. During El Niño events, reduced precipitation and increased evaporation can elevate salinity and weaken stratification, facilitating more efficient vertical mixing when strong monsoonal winds are present. This preconditioning may enhance thermocline shoaling and biological productivity relative to neutral years. An additional key aspect is the time lag between physical forcing and biological response. While SST cooling and thermocline uplift occur rapidly in response to wind forcing, phytoplankton growth depends on sufficient nutrient accumulation within the euphotic zone. The gradual increase in chlorophyll from June to August indicates nutrient buildup followed by biological utilization, a pattern characteristic of monsoon-driven upwelling systems.

These findings underscore the need to integrate physical indicators (SST, thermocline depth, EPV) with biogeochemical indicators (chlorophyll distribution) to reliably identify upwelling processes. While SST cooling alone may result from air–sea heat flux variability, its concurrence with negative EPV, thermocline shoaling, and chlorophyll enhancement strengthens the interpretation of wind-driven upwelling. From a broader perspective, upwelling variability in the Arafura Sea has significant implications for marine ecosystems and fisheries productivity. Increased nutrient supply during periods of intensified upwelling may enhance primary productivity and support higher trophic levels. However, the observed interannual variability indicates that this productivity fluctuates in response to the interaction between monsoon strength and ENSO variability.

In summary, these results demonstrate that upwelling variability in the southwestern Arafura Sea is primarily governed by the interplay of seasonal monsoon forcing, Ekman

dynamics, and interannual climate variability. The consistent associations among wind intensity, Ekman transport, SST variability, thermocline depth, and chlorophyll response underscore the critical role of atmosphere–ocean coupling in regulating both the physical structure and biological productivity of the Arafura continental shelf.

4. Conclusions

Upwelling variability in the southwestern Arafura Sea demonstrates marked seasonal dependence, primarily controlled by monsoonal wind forcing and Ekman dynamics. During the Southeast Monsoon, negative Ekman Pumping Velocity (EPV) dominates the southern region, promoting coastal upwelling through offshore Ekman transport. In contrast, the Northwest Monsoon reverses ocean dynamics, leading to downwelling in the southwestern region and upwelling in the northeastern region. These findings suggest that the study area serves as a transition zone between the coastal Arafura Sea system and the broader Banda Sea circulation. Therefore, upwelling variability is shaped by both local wind forcing and regional basin-scale circulation.

On the interannual timescale, El Niño–Southern Oscillation (ENSO) variability further modulates the intensity of upwelling processes. El Niño events generally enhance upwelling signals through stronger Southeast Monsoon winds and increased Ekman transport, whereas La Niña events tend to suppress these processes. Overall, the results demonstrate that upwelling formation in the study area is determined by the combined influences of monsoonal wind forcing, regional circulation dynamics, and climate variability, each of which affects sea surface temperature variability and biological productivity. These findings highlight the importance of monsoon–ocean interactions in determining the physical structure and ecosystem productivity of the Arafura Sea and provide valuable insights into regional oceanographic variability.

Conflicts of Interest

There are no conflicts to report.

Acknowledgements

The author expresses gratitude to INPEX Masela Ltd. for the CTD data, which are part of the ocean survey for the development of the Abadi Field, as well as academic supervisors for their support during the research process, and appreciates colleagues and partners who provided insights throughout the analysis and manuscript preparation.

AI Writing Statement

During the preparation of this work, the author(s) used ChatGPT to check the coherence of the translated sentences and Grammarly to review grammatical accuracy. After using this tool/service, the author(s) reviewed and edited the content as needed and takes full responsibility for the content of the publication.

References

Arisandi, R.C., Jumarang, M.I., & Apriansyah. (2017). Variabilitas Suhu dan Salinitas Perairan Selatan Jawa Timur. *Prisma Fisika*, *V*(3), 131-137.

Atmadipoera, A.S., Almatin, A.A., Zuraida, R., & Permanawati, Y. (2020). Seasonal upwelling in the northern Arafura sea from multidatasets in 2017. *Pertanika Journal of Science and Technology*, *28*(4), 1487-1515. https://doi.org/10.47836/pjst.28.4.19

Bernades, H., Suryoputro, A.A.D., Wirasatriya, A., Handoyo, G., Rifai, A., Maslukah, L., & Sugianto, D.N. (2021). The effect of Ekman mass transport and Ekman pumping velocity on the variability of sea surface temperature in the Arafura Sea. *IOP Conference Series: Earth and Environmental Science*, *919*(1). https://doi.org/10.1088/1755-1315/919/1/012026

Buton, I., Tubalawony, S., & Wattimena, M.C. (2023). Variabilitas Hidrometeorologi Permukaan Laut Arafura Pada Saat Fenomena Enso. *Jurnal Laut Pulau: Hasil Penelitian Kelautan*, *2*(2), 32-50. https://doi.org/10.30598/jlpvol2iss2pp32-50

Clark, C.O., Cole, J.E., & Webster, P.J. (2000). Indian Ocean SST and Indian Summer Rainfall: Predictive Relationships and Their Decadal Variability. *Journal of Climate*, *13*(14), 2503-2519. https://doi.org/10.1175/1520-0442(2000)013<2503:IOSAIS>2.0.CO;2

Kämpf, J. (2015). Undercurrent-driven upwelling in the northwestern Arafura Sea. *Geophysical Research Letters*, *42*(21), 9362-9368. https://doi.org/10.1002/2015GL066163

Kämpf, J., & Chapman, P. (2016). Upwelling Systems of the World. In *Upwelling Systems of the World*. https://doi.org/10.1007/978-3-319-42524-5

Kida, S., & Wijffels, S. (2012). The impact of the Indonesian Throughflow and tidal mixing on the summertime sea surface temperature in the western Indonesian Seas. *Journal of Geophysical Research: Oceans*, *117*(C9). https://doi.org/10.1029/2012JC008162

Pranowo, W.S. (2012). Dinamika Upwelling dan Down Welling Di Laut Arafura dan Timor. *Widyariset*, *15*, 415-424.

Rachman, H.A., Gaol, J.L., & Syamsudin, F. (2019). Variasi Data Suhu Permukaan Laut, Tinggi Paras Laut, Klorofil-a, dan Upwelling di Perairan Selatan Jawa serta Korelasinya Dengan Data Lapangan. *Journal of Marine and Aquatic Sciences*, *5*(2), 289. https://doi.org/10.24843/jmas.2019.v05.i02.p17

Ramadyan, F., & Radjawane, I.M. (2013). Seasonal Surface Geostrophic Current in Arafura-Timor Waters. *Jurnal Ilmu Dan Teknologi Kelautan Tropis*, *5*(2), 261-272. https://doi.org/10.29244/jitkt.v5i2.7556

Ratnawati, H.I., Hidayat, R., Bey, A., & June, T. (2016). Upwelling di Laut Banda dan Pesisir Selatan Jawa serta Hubungannya dengan ENSO dan IOD. *Omni-Akuatika*, *12*(3), 119-130. https://doi.org/10.20884/1.oa.2016.12.3.134

Rudiastuti, A.W., Gaol, J.L., & Nurjaya, I.W. (2007). *Distribusi Klorofil-a dari citra MODIS dan hubungannya dengan aktivitas kapal penagkap ikan dari Vessel Monitoring System. Kumpulan Riset Kelautan: Menuju Sumber Daya Alam Yang Lestari* (p. 274). Bogor, Indonesia: Pusat Survei Sumber Daya Alam Laut-BAKOSURTANAL.

Talley, L.D., Pickard, G.L., Emery, W.J., & Swift, J.H. (2011). *Descriptive Physical Oceanography An Introduction* (6th ed.). London, United Kingdom: Academic Press. https://doi.org/10.1016/B978-0-7506-4552-2.10001-0

Wattimena, M.C., & Tubalawony, S. (2023). Variasi Parameter Oseanografi di Utara Laut Arafura pada Tahun Super La Nina 2010 dan El Nino 2015. *Journal of Coastal and Deep Sea*, *1*(1), 42-50. https://doi.org/10.30598/jcds.v1i1.11325

Wirasatriya, A., Setiawan, J.D., Sugianto, D.N., Rosyadi, I.A., Haryadi, H., Winarso, G., Setiawan, R. Y., & Susanto, R.D. (2020). Ekman dynamics variability along the southern coast of Java revealed by satellite data. *International Journal of Remote Sensing*, *41*(21), 8475-8496. https://doi.org/10.1080/01431161.2020.1797215